IOP Publishing Semiconductor Science and Technology
Semicond. Sci. Technol. **36** (2020) 015002 (10pp) https://doi.org/10.1088/1361-6641/abbba8

Performance improvement of ultrasonic spray deposited polymer solar cell through droplet boundary reduction assisted by acoustic substrate vibration

Sobia Waheed, Saurabh Pareek, Punit Sharma and Supravat Karak

Organic and Hybrid Electronic Device Laboratory (OHEDL), Centre for Energy Studies, Indian Institute of Technology Delhi, New Delhi 110016, India

E-mail: supravat@ces.iitd.ac.in

Received 14 August 2020, revised 23 September 2020
Accepted for publication 25 September 2020
Published 22 October 2020

Abstract

This study demonstrates the performance improvement of ultrasonic spray deposited bulk heterojunction type polymer solar cells through droplet boundary reduction assisted by acoustic substrate vibration of varying frequencies between 0–20 kHz. The optimum performance was achieved at 15 kHz of applied frequency, where ∼68% improvement in short-circuit current density and ∼85% improvement in overall cell efficiency were observed compared to the reference devices fabricated on stationary substrates. The performance enhancement is mainly attributed to the improved film morphology due to uniform and homogenous droplet spreading and coalescence under the influence of acoustic vibration. Systematic improvement was observed until 15 kHz when smooth films with significantly reduced droplet boundaries were observed with surface roughness around 10 nm only. However, beyond this point, higher frequencies were found to have detrimental effect on film formation. Significant improvement was observed for every cell parameter for 15 kHz samples. Almost ∼16% enhancement in carrier generation rate and ∼46% enhancement in exciton dissociation probability were observed, as estimated from the photo-current analysis. Urbach energy estimation reveals that the films, prepared at 15 kHz substrate vibration, forms less amount of band edge localized defect states ($E_{u\ (no\ vibration)} = 161$ meV and $E_{u\ (15\ kHz)} = 120$ meV), resulting into reduced non-radiative recombination and better performances. The presented approach opens up new pathways for uniform and scalable thin film growth through acoustic substrate vibration assisted ultrasonic spray deposition technique, which would be beneficial for large scale industrial organic photovoltaic production.

Supplementary material for this article is available online

Keywords: organic photovoltaic, ultrasonic spray, acoustic vibration, photocurrent, Urbach energy

(Some figures may appear in colour only in the online journal)

1. Introduction

Conjugated polymers have gained tremendous attention in the past few decades owing to their mechanical flexibility, lightweight and solution processability [1]. On combining two conjugated polymers or small molecules with different electron affinity (electron-donor and electron-acceptor), bulk-heterojunction (BHJ) can be formed, which has attracted broad research attention particularly in the field of organic photovoltaic (OPV) [2–4]. Such devices are promising for next

generation low cost solar energy harvesting due to their compatibility with high-throughput roll-to-roll (R2R) processing. OPVs have recently achieved remarkable power conversion efficiency (PCE) approaching 18% for single junction devices [5] and 26% under room lighting [6] using various novel molecular and device engineering approaches [7–9]. However, such results are generally limited to laboratory level experiments, typically employing small scale coating methods like spin coating and drop casting. To follow the footprint of Si solar cells to their successful commercialization, the future of the OPV industry depends on the development of solution processable and scalable deposition techniques. It is one of the major research thrusts now to achieve the OPV device performances via deposition techniques like gravure printing, inkjet printing, screen printing, slot-die casting, or spray coating, similar to the spin coated small scale champion devices [10–15].

Among these techniques, spray coating possesses the potential to realize scalable R2R manufacturing of OPV devices as it is a low wastage, high through-put, cost effective, and solution processed deposition method [16–19]. The technique utilizes a dilute solution of the material to be deposited, which passes through a nozzle. The nozzle breaks the solution into small droplets via the process called 'atomization' [20–22]. These atomized droplets travel away from the nozzle with airstream and impact on the surface. The droplets then spread and coalesce with one another, forming a thin liquid film. The spray process distinguishes itself from other deposition techniques by facilitating the film deposition of desired thickness, layer by layer deposition and its flexibility in substrate independent patterning. Despite the advantages, spray deposited films often contain pinholes, entrapped air-bubbles, rigid droplet boundaries and poor material crystallinity, limiting the device performances. Fundamental understanding of the growth mechanism and influences of various spray parameters on film morphology are still lacking which is crucial for efficient device fabrication [23]. Various attempts have been made to overcome these challenges by the pre/post- annealing treatment [24–26], solvent annealing [27–29] and excitation by substrate vibration [30].

Recently high frequency vibrations have been used for the synthesis of crystalline materials and powders from molten metals [31, 32]. Eslamian *et al* [33–42], have shown that by applying ultrasonic vibration on thin films better uniformity and electrical properties can be achieved. They have demonstrated that thin films treated by low power ultrasonic vibration during or after deposition exhibit significant enhancement in overall film quality due to the creation of fluid flow phenomenon like microstreaming (swirling motion inside the liquid), surface waves (waves generated at the liquid-air interface), liquid evaporation along with acoustophoresis (a force applied by acoustic waves on particles suspended in the liquid). For drop casting and spray coating processes [33–35], substrate vibration found to facilitates surface wetting, droplet spreading and coalescence in a similar manner. However, at the same time with an increase in power the substrate vibration found to impose a detrimental effect on the film quality too by destabilization, causing 'dewetting' and droplet breakup. With several reports on the application of vibration on thin film growth, the opportunities to expand the understanding of its fundamental mechanism for device applications are flourishing.

In our previous report [26], one to one correlation between spin coated and ultrasonic spray coated P3HT:$PC_{71}BM$ based OPV devices were carried out and it was demonstrated that by applying *in-situ* annealing simultaneously during the film growth at a temperature lower than the solvent boiling point, significant control can be achieved over the nanoscale film morphology leading to comparable device efficiencies. However, it was also surmised that *in-situ* annealing alone could not eliminate all the droplet boundaries which possess performance limitations and it was suggested that higher efficiency can be achieved by further minimizing such droplet boundaries. This work is an extension of our previous work toward this particular aspect with the same material system used before. Here, we have applied acoustic vibration with varying frequencies on the substrate during spray deposition of the P3HT:$PC_{71}BM$ solution and have studied various effects of vibration frequencies on film morphology and photovoltaic performances. To the best of our knowledge, we are unaware of any such experimental studies on the effect of vibrational frequencies on the device performance so far. Additionally, in most cases, ultrasonic vibration has been utilized for excitation of the thin liquid film, which generally requires expensive piezoelectric sources. In comparison, acoustic sources are cost effective, robust and easily compatible with any R2R setup. Systematic investigations were carried out to understand various effects of substrate vibrations on active layer film morphology and optoelectronic properties of the spray deposited P3HT:$PC_{71}BM$ film, which enabled us to identify the key factors for performance improvement.

2. Experimental details

2.1. Materials

The polymers (P3HT (98% regioregular,) and $PC_{71}BM$ (99%)) were obtained from 1-material. Poly (3, 4-ethylene dioxythiophene): poly(styrenesulfonate) (PEDOT: PSS) (1.3 wt% dispersion in H_2O, conductive grade), Chlorobenzene (HPLC, 99.9%) and Lithium Fluoride (LiF) were purchased from Sigma Aldrich.

2.2. Method

The ITO coated glass substrates were cleaned by ultrasonication in deionized water, soap solution, acetone and isopropanol for 20 min at each step, followed by vacuum drying and UV-Ozone treatment for 20 min. The treated substrates were immediately transferred for spin coating of PEDOT:PSS (filtered through a 0.45 μm filter before deposition) at 3500 rpm for 60 s and were baked at 150 °C for 15 min in air. A solution of P3HT:$PC_{71}BM$ (1:1) was prepared by dissolving in chlorobenzene with a material concentration of 3 mg ml^{-1} and stirred for 12 h. The ultrasonic spray deposition was performed on the prepared ITO/PEDOT:PSS

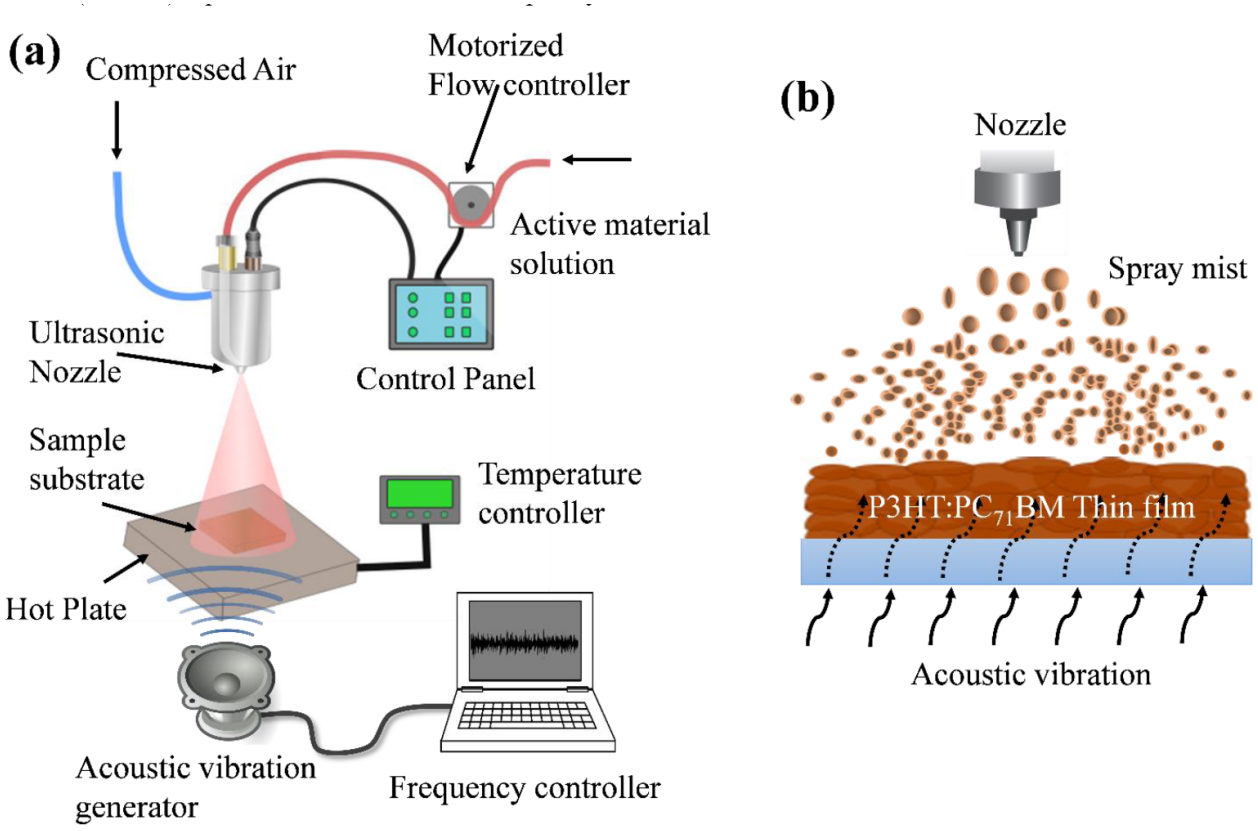

Figure 1. (a) Setup for ultrasonic spray deposition on a vibrating substrate, (b) the applied vibration facilitates further coalescence.

substrates at 80 °C *in-situ* annealing condition with the substrate to nozzle distance of 19 cm, air pressure of 20 psi, the flow rate of 1.5 ml min^{-1}. A computer-controlled audio source was placed under the substrate stage to generate the acoustic waves and was fed with 3 dB sinusoidal signals of variable frequencies. Except for the vibration frequency, all other coating parameters, as described in our previous work [26], were kept unchanged throughout the study to understand the effect of substrate vibration on film properties and device performances separately. The schematic diagram of the setup is shown in figure 1(a). After spray deposition of the films, before transferring them to the thermal evaporation chamber, all samples were post annealed at 120 °C for 20 min under N_2 atmosphere. The thin layer of LiF (1 nm) and Al (100 nm) top electrodes were then subsequently deposited through thermal evaporation under high vacuum ($\sim 10^{-6}$ mbar). The final devices have the conventional structure of ITO/PEDOT:PSS (50 nm)/P3HT:PC_{71}BM active layer (200 nm)/LiF(1 nm)/Al (100 nm) with a device area of 2 × 2 mm^2.

2.3. Characterization

To investigate the effect of vibration on thin film and photovoltaic characteristics, several methods were employed. The wide view optical microscopic images of the surface of the as deposited active layers were captured by Olympus BX53M microscope. Nanoscale morphology and surface roughness were investigated using Bruker Dimension Icon AFM with Scan Asyst under tapping mode. The optical characteristics of spray deposited films were studied using photoluminescence spectra from Edinburgh Instruments FLS920 Fluorescence spectrophotometer and the UV–VIS-NIR absorption spectrophotometer of Perkin Elmer Lambda-1050. The Impedance Spectroscopy (IS) measurements were done through NF corporation-ZM2376 LCR meter. The x-ray diffraction patterns were obtained using a Rigaku ultima-IV x-ray Diffractometer using Cu-Kα radiation (λ = 1.54 Å). The photovoltaic characteristics were measured using Keithley 2401 source meter with AAA solar simulator with AM 1.5G solar spectrum under stimulated radiation condition of 76.2 mW cm^{-2}.

3. Results and discussion

Figure 1(a) shows the schematic diagram of the deposition set up. The blend solution of P3HT:PC_{71}BM was feed through the nozzle where ultrasonic vibration and compressed air were used for atomization of the solution. All process parameters were controlled by the digital control panel and the hot stage temperature was precisely set at 80 °C using a PID controller. The substrate vibration was generated and varied between 0–20 kHz using a computer controlled acoustic source. As shown in figure 1(b), we anticipate that the fine mist of active solution, generated by the ultrasonic spray nozzle, will reach the hot substrate while it is vibrating in tune with the different acoustic frequencies. After impact with the substrate, the acoustic energy will get transmitted to the falling

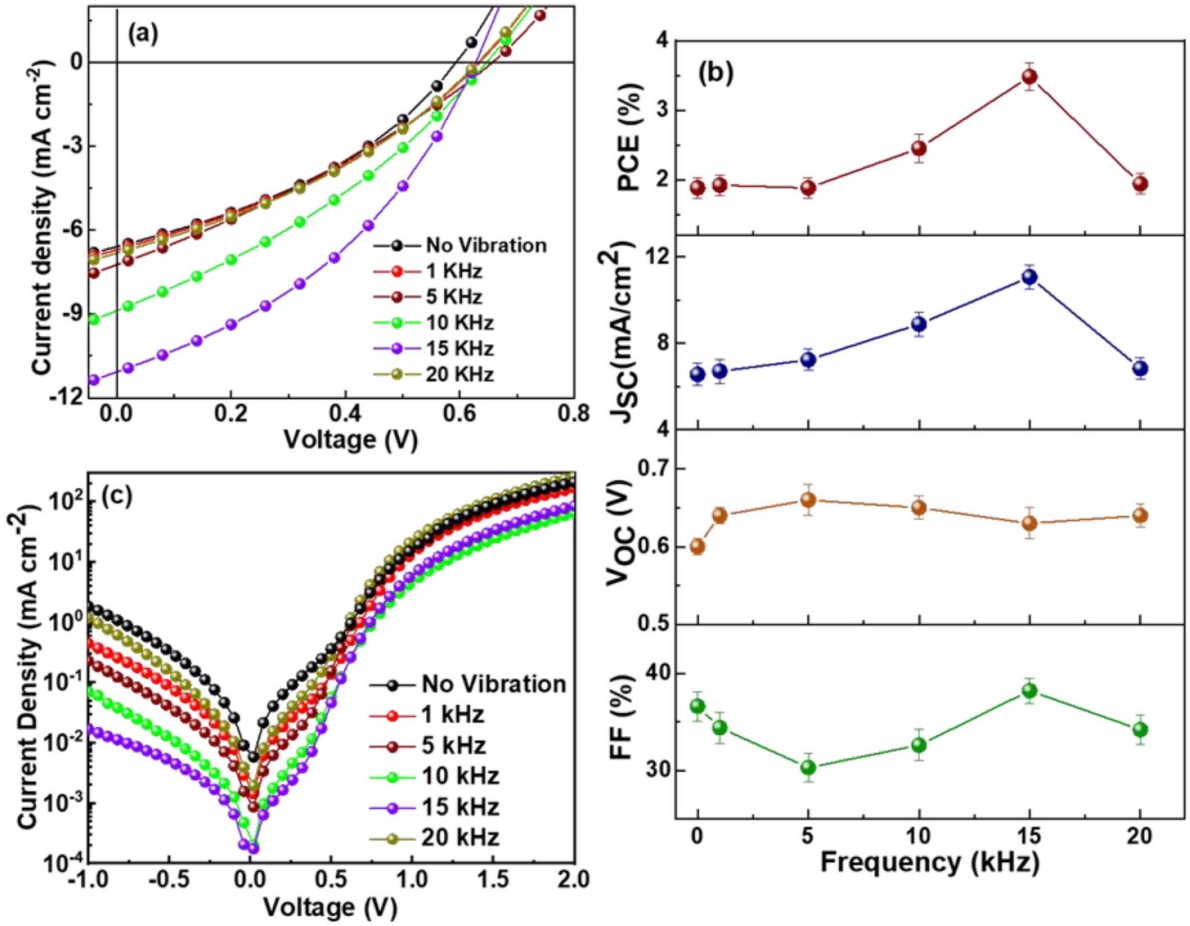

Figure 2. (a) J–V characteristics of ultrasonic spray coated devices prepared at various acoustic substrate vibration under AM 1.5 solar radiation, (b) photovoltaic parameter variations and (c) dark J–V characteristic of the corresponding devices.

droplets, generating surface waves and fluid forces. This will in turn lead to enhanced droplet spreading and coalescence of the impinging droplets [40] while the substrate temperature (*in-situ* annealing at 80 °C) will facilitate simultaneous drying of the film to prevent any droplet retraction. Therefore, uniform and homogeneous coating of the film is expected with much reduced droplet boundaries which are extremely crucial for device performances. Various experiments were performed to investigate the effects of substrate vibration on film morphology and corresponding device performances to identify the key limiting factors and threshold point for such novel deposition technique as discussed below.

3.1. Photovoltaic performance

The photovoltaic performance of the devices, prepared at different substrate vibrations, were compared by measuring their current density (J) vs. voltage (V) characteristics under AM 1.5G simulated solar radiation condition as presented in figure 2(a). Figure 2(b) and table S1 (available online at https://stacks.iop.org/SST/36/015002/mmedia) (supporting information) summarized the detailed variations of different photovoltaic parameters like power conversion efficiency (PCE), short circuit current density (J_{sc}), open circuit voltage (V_{oc}) and fill factor (FF) for the corresponding devices. Devices prepared on stationary substrates without any vibration exhibit a short circuit current density (J_{sc}) of 6.57 mA cm^{-2}, an open circuit voltage (V_{oc}) of 0.59 V and FF of 36.6%, resulting in PCE of 1.88%. With the introduction of acoustic substrate vibration, gradual improvements were observed for J_{sc}, FF and PCE, while V_{OC} remains almost the same. Devices fabricated at 15 kHz substrate vibration showed best performances with PCE $\sim$ 3.48% which is almost 85% higher than the reference devices, with J_{sc} of 11.07 mA cm^{-2}, V_{oc} of 0.63 V and FF of 38.2%. This can be attributed to improved film morphology and surface coverage [36, 39]. Device performances were found to get deteriorate beyond this point, possibly due to the detrimental effects of higher frequencies on film morphology. To understand the effect of substrate vibration on device operation further, their corresponding dark J–V characteristic were also investigated as shown in figure 2(c). Interestingly, devices showed gradually reduced leakage current in the reverse bias region with increasing substrate vibration, compared to the reference devices (no vibration). The highest rectification ratio of $\sim 10^3$ at ± 1 V was observed for the devices prepared at 15 kHz substrate vibration while devices with higher substrate vibration (20 kHz) showed significantly large leakage current. This again indicates that after a threshold

point higher frequencies are having detrimental effects on film morphology, possibly causing splashing and droplet breaking, thus providing parasitic leakage paths for the charge carriers.

3.2. Active layer morphology

Optical microscope and AFM imaging have been used to understand the evolution of the active layer film morphology with the applied acoustic substrate vibrations. Optical microscope images were recorded for an average area of 250 μm $\times$ 200 μm at several different locations on the surface of the films prepared at different substrate vibration conditions, as shown in figure 3. It is evident that substrate vibrations have significant influences over film morphology in terms of droplet spreading and coalescence effects. Films deposited on stationary substrates (figure 3(a)) showed visible concentric and overlapped circles, i.e. rigid droplet boundaries, indicating restricted droplet spreading and merging in their liquid state leading to non-uniform film formation. Interestingly, with the application of substrate vibration, even under the influence of moderate acoustic frequencies the boundaries seem to be reduced significantly, while at 15 kHz of the applied frequency the surface looks almost continuous without any visible droplet boundary. However, in the case of 20 kHz, high frequency found to cause excessive agitation and re-coarsening of droplets [36], making the films non-uniform again. Such nanoscale alteration of film morphology is extremely crucial for conjugated polymer blend films as it largely controls the OPV performances.

This is also evident from the AFM images as shown in figure 4. The RMS roughness of the films was found to get significantly decreased with the introduction of substrate vibration. It should be noted that films deposited by spray, showed usually higher roughness due to the peaks and valleys made by droplet boundaries. Therefore, the area chosen for roughness measurement becomes often crucial. In this study, an average area of 50 μm $\times$ 50 μm was chosen at multiple locations of the films to ensure that it includes the droplet boundary and the crater sufficiently to avoid any artefacts. The films prepared at no vibration condition showed very high surface RMS roughness of about 100 nm due to the presence of a large number of rigid droplet boundaries as observed in microscopic images. The RMS roughness has instantly reduced to 90 nm after the application of substrate vibration with just 1 kHz of acoustic frequency. The substrate vibration seems to have smoothened the film to some extent by filling the valleys compared to the films prepared at the no-vibration condition. The film roughness got further reduced to 60 nm and 30 nm for 5 kHz and 10 kHz, respectively. The optimum film quality was obtained at 15 kHz while RMS roughness of about $\sim$10 nm was observed which is almost comparable with spin coated films. However, at 20 kHz the roughness has again increased (90 nm) probably due to the excessive perturbation. This is fairly consistent with our corresponding device results and explained the improved performances at 15 kHz of substrate vibration.

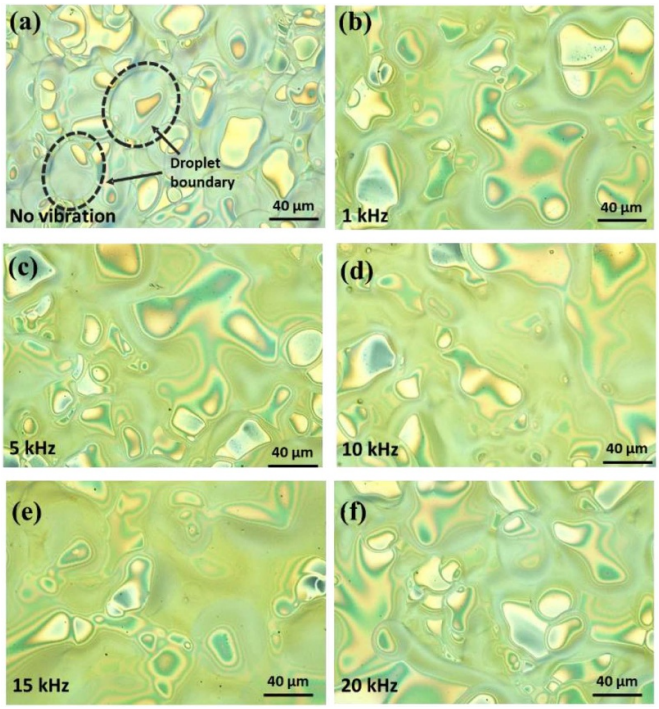

Figure 3. Optical microscope images of ultrasonic spray deposited P3HT:$PC_{71}BM$ film at different acoustic vibration frequencies (a) no vibration, (b) 1 kHz, (c) 5 kHz, (d) 10 kHz, (e) 15 kHz, and (f) 20 kHz.

3.3. Optoelectronic properties

Various influences of substrate vibration on the optical properties of the films were investigated by UV–Vis–NIR absorption spectroscopy. Figure 5(a) showed the total reflection spectrum of the films. It is interesting to note that although the overall features of the reflection spectrum remain almost similar for all the films, slight changes in the magnitude of the total reflection was observed. The total reflection of the films found to get increased up to the applied frequency of 15 kHz, suggesting an improvement in surface flatness until this frequency and then getting degraded at a higher frequency again. These results are in good agreement with our previous observation suggesting that the acoustic vibration of 15 kHz is beneficial for uniform and homogeneous film deposition. The absorption spectra of the corresponding films are shown in the inset of figure 5(a). All the films showed broadband absorption capabilities with peaks at 510 nm and 550 nm and a shoulder peak at 600 nm attributed to crystalline P3HT structure correspond to the (0–2), (0–1) and (0–0) transition, respectively. However, the overall absorption capability for all the films seems to be unaffected by acoustic vibration. This indicates that there are negligible changes in polymer band structure or chain alignment due to the substrate vibration during film growth. This has been further verified by XRD analysis of the films as shown in figure S1 in supporting information. No significant variations were observed in P3HT crystallinity. Therefore it can be safely concluded that while *in-situ* annealing is primarily controlling film crystallinity, polymer chain orientations, π–π

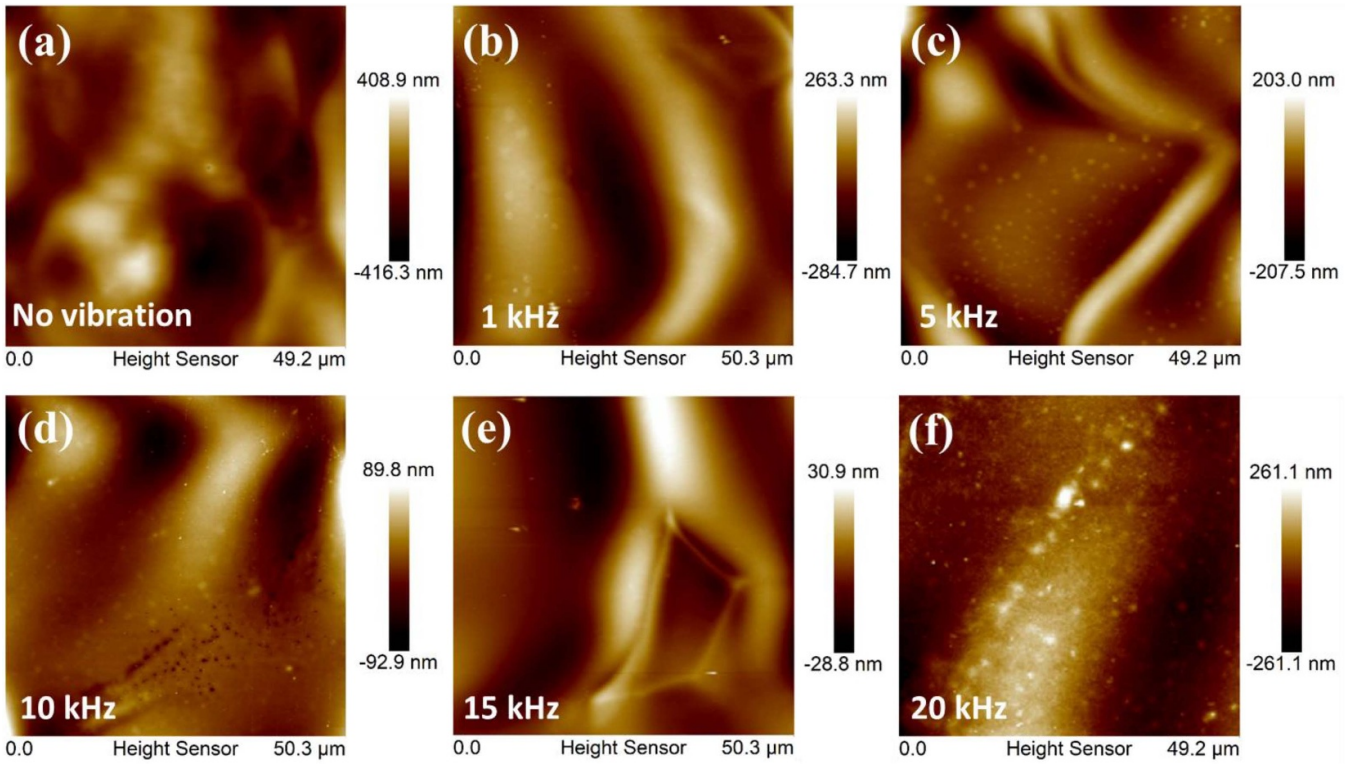

Figure 4. AFM images of the ultrasonic spray deposited films at different acoustic vibration frequencies (a) no vibration, (b) 1 kHz, (c) 5 kHz, (d) 10 kHz, (e) 15 kHz, and (f) 20 kHz.

stacking, etc [26], the substrate vibration is providing additional control over the film uniformity, homogeneity, roughness and rigid droplet boundary. As polymers are generally soft disordered materials, such alteration in film morphology should in turn affect the localized defect states in the blend films. To investigate the effect of substrate vibration on defect state formation, Urbach energy analysis was performed for P3HT:$PC_{71}BM$ blend active layers spray coated at no vibration and 15 kHz substrate vibration conditions, as shown in figure 5(b). Urbach energy (E_u), which directly correlates the quantitative measures for defect formation for disordered semiconducting materials [43, 44], can be calculated from the slope of the exponential tail of the absorption coefficient (α) *vs.* photon energy ($h\nu$) plot by using the following linear equation [44];

$$\alpha = \alpha_0 \exp\left(\frac{h\upsilon - h\upsilon_0}{E_u}\right) \quad (1)$$

where h is Planck's constant and α_0, ν_0 and E_u are fitting parameters. As evident from figure 5(b), the tail broadening for the samples prepared at 15 kHz substrate vibration has significantly reduced as compared to the reference samples prepared at no vibration condition, suggesting a reduction in defect states for the films under the influence of acoustic substrate vibration. The estimated Urbach energy was found to be around ~161 meV for the reference samples while it reduced to ~120 meV for 15 kHz sample. Such a significant drop (almost ~25%) in Urbach energy indicates that substrate vibration is successfully reducing the localized defect states in the active layer films, possibly by a reduction in rigid droplet boundaries as evident from our microscope and AFM images. This should have a major impact on charge carrier transport and non-radiative recombination of photogenerated charge carriers into the active layer of the devices. Therefore, it can be attributed that the lower Urbach energy could be one of the possible reasons for the observed increase in PCE for the OPV device prepared at 15 kHz substrate vibration.

3.4. Photogenerated charge carrier dynamics

To understand the impact of morphology evoluation under substrate vibration on photogenerated charge carrier dynamics of the devices, exciton generation rate (G_{max}) and dissociation probability (P) have been analysed by comparing their net photocurrent density (J_{PH}) vs. effective bias voltage (V_{eff}) dependencies as shown in figure 6(a). The net photocurrent density J_{PH} can be considered as the difference between total photocurrent density J_L and dark current density J_D, i.e. $J_{PH} = J_L$-J_D. Whereas, the effective bias voltage V_{eff} can be defined as ($V_0 - V$), where, V is the applied voltage and V_0 is the voltage at which there is no photocurrent in the device ($J_{PH} = 0$) [3, 45]. At small effective voltage, linear increment in J_{PH} was observed with V_{eff}, suggesting that the photocurrent is dominated by diffusion of charge carriers at this point under low electric field, while at higher V_{eff} region, the J_{PH} started to get saturated dominated by the drift of the charge carriers. Both diffusion and drift regions were evident for all the devices. The maximum carrier generation rate can be estimated from the magnitude of the saturated photocurrent (J_{PH_sat}) at the drift

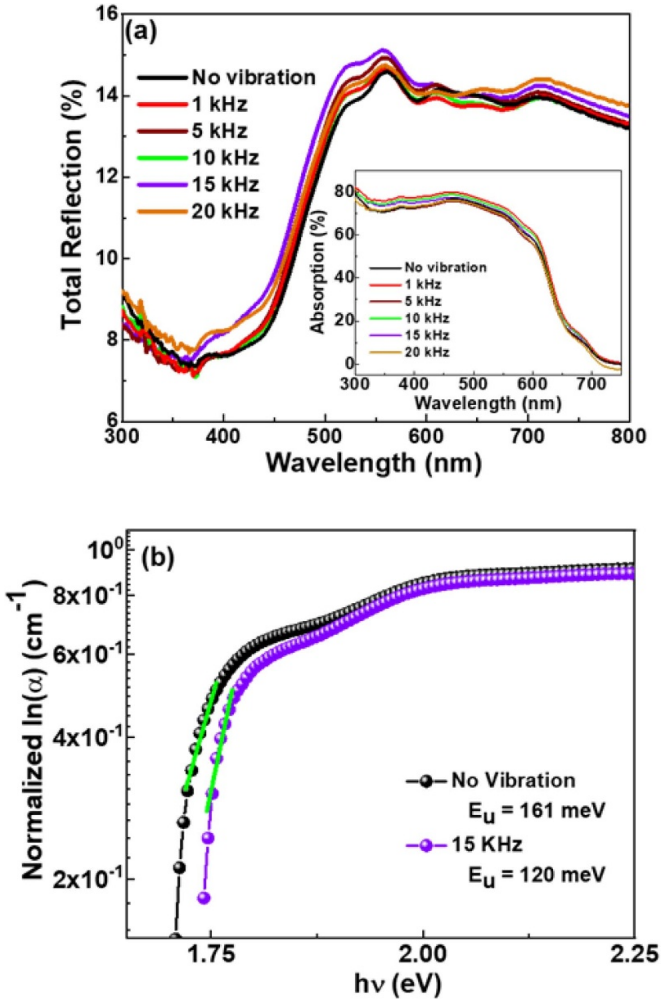

Figure 5. (a) Total reflection spectra of the films prepared at different substrate vibrations; Inset: their corresponding UV–Vis absorption spectra, (b) Urbach energy estimation by fitting exponential tail in absorption vs. photon energy plot for samples prepared at reference (no vibration) and optimal (15 kHz) conditions.

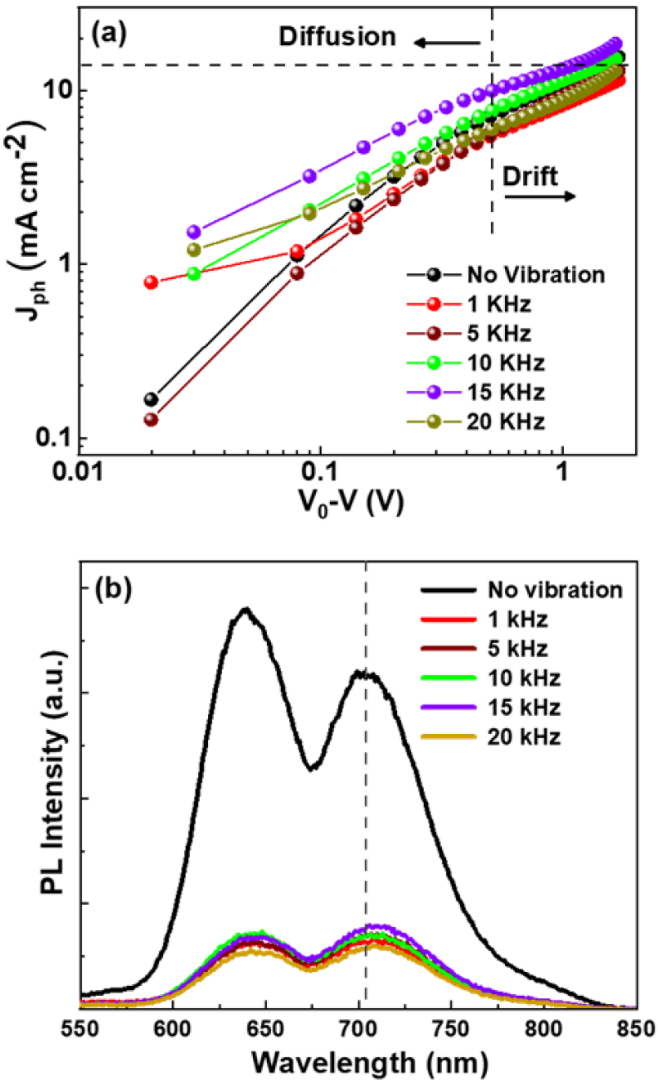

Figure 6. (a) Photocurrent density (J_{PH}) vs. effective voltage (V_{eff}) of the devices prepared at different substrate vibrations (b) Photoluminescence spectra of P3HT:PC_{71}BM blend films deposited at different substrate vibrations.

region where exciton dissociation and charge carrier extraction are taking place simultaneously due to the high built-in electric field. The maximum generation rate can be expressed as [46]:

$$G_{\max} = \frac{J_{PH\_sat}}{eL} \tag{2}$$

where e and L represent the electric charge and the thickness of the active layer. The maximum generation rate for the reference devices (no vibration) was found to be $\sim 4.75 \times 10^{21}$ cm^{-3} s^{-1} whereas, for the optimum devices prepared at 15 kHz substrate vibration, it was found to be $\sim 5.52 \times 10^{21}$ cm^{-3} s^{-1}, which is almost $\sim$16% higher compared to the reference one. Similarly, $\sim$46% improvement in the exciton dissociation probability, which can be estimated from the ratio of photocurrent density and saturated photocurrent density, was also observed for the 15 kHz samples compared to the reference one. The dissociation probability is found to be $\sim$83.54% for 15 kHz devices, whereas for the reference devices it is around $\sim$57.63% only. This could lead to a significant reduction in non-radiative carrier recombination for the devices prepared at 15 kHz substrate vibration which we believe is one of the primary reasons for their improved performances. It should be noted that the 15 kHz samples are also having a lesser amount of active layer localized defect states compared to the reference samples, as evident from the Urbach energy estimation, which is in good agreement with their higher exciton generation-dissociation properties. This is mainly because of the fact that the introduction of substrate vibration assists the liquid droplets for uniform spreading and coalescence creating homogeneous films with reduced rigid droplet boundaries and trap states. As the nanoscale morphology largely controls the mobility of charge carriers for polymer based BHJ films, it should directly impact the charge transport properties of our devices as well. The same has been investigated by impedance spectroscopy as shown in figure

S2 and table S2 in the SI. The value of transport resistance (R2) decreased from 3.32 kΩ cm^2 for no vibration to a minimum value of 735 Ω cm^2 for the 15 kHz samples, indicating improved charge transport efficiency of the devices. Similarly, almost three orders of reduction in diffusion time (τ_d) from 196 ms to 604 μs and almost three orders increment in zero bias dark mobility from 7.9 × 10^{-12} cm^2 V^{-1} s^{-1} to 2.6 × 10^{-9} cm^2 V^{-1} s^{-1} were observed for 15 kHz devices compared to reference (no vibration) devices. Considering the fact that all the devices were prepared with identical deposition parameters except for substrate vibration frequency, the difference in response is likely due to the modification in interfaces and bulk of the BHJ layer. This is in good agreement with the other findings, further confirming the novelty of the proposed approach.

The individual photoluminescence (PL) spectra of P3HT and its blend film with $PC_{71}BM$ (reference sample) were shown in figure S3 in SI, while the PL spectra correspond to the P3HT:$PC_{71}BM$ blend films deposited at various vibration conditions are shown in figure 6(b). All the samples showed more than 98% PL quenching confirming efficient photo-induced charge transfer between donor–acceptor phases. Two distinct peaks were observed for the reference sample, one around 641 nm associated with 0–0 emission and the other around 703 nm associated with 0–1 emission [47, 48]. Increased PL quenching was observed for the films prepared on vibrating substrates, possibly due to better mixing of donor and acceptor materials under the influence of acoustic vibration [49]. A slight redshift can also be observed in the 0–1 emission peak, perhaps indicating improved polymer aggregation.

4. Conclusion

In conclusion, we have successfully demonstrated that by introducing acoustic substrate vibration film morphology and photovoltaic performances can be greatly controlled for ultrasonic spray coated OPVs. Various effects of substrate vibration on active layer phase segregation and optoelectronic properties of the devices have been investigated in detail. The results suggest that acoustic vibration significantly assists the liquid droplets for uniform spreading and coalescence forming homogeneous films with a roughness of as low as 10 nm by reducing rigid droplet boundaries. The photovoltaic parameters of the devices have successfully improved up to 15 kHz of substrate vibration, compared to the reference devices. An 85% improvement in overall cell efficiency and 68% improvement in short-circuit current density was observed for the optimal devices. The Urbach energy analysis indicates that films prepared at 15 kHz have relatively less amount of localized defect states ($E_{u\ (no\ vibration)}$ = 161 meV and $E_{u\ (15\ kHz)}$ = 120 meV), compared to the films prepared on stationary substrates. The acoustic vibration induces synergic improvement in both carrier generation, exciton dissociation as well as charge carrier transportation. From photocurrent investigations, it was found that the maximum carrier generation rate has increased from 4.75 × 10^{21} cm^{-3} s^{-1} to 5.52 × 10^{21} cm^{-3} s^{-1} while exciton dissociation probability has also increased from 57% to 84% for the champion devices prepared at 15 kHz, as compared to the reference samples. Impedance measurement indicates three orders of improvement in dark mobility, diffusion time and transport resistance for the corresponding devices. PL measurement confirms ultrafast photo-induced charge transfer capabilities of the devices. Devices prepared on vibrating substrates showed higher PL quenching, indicates better donor–acceptor phase mixing under the influence of acoustic vibration. Our results offer a novel approach for state-of-art device fabrication by scalable ultrasonic deposition technique which can be applied for a variety of materials for developing large area efficient OPV devices.

Acknowledgments

We would like to thank Science and Engineering Research Board, Department of Science and Technology (Project no. ECR/2017/000152) and DST-INSPIRE Fellowship program for financial support. We are also thankful to Nanoscale Research Facility and Central Research Facility, Advanced materials and photovoltaic device laboratory, IIT Delhi for the characterization facilities.

ORCID iDs

Sobia Waheed https://orcid.org/0000-0002-1262-4385
Saurabh Pareek https://orcid.org/0000-0002-0461-9930
Supravat Karak https://orcid.org/0000-0002-0650-8353

References

[1] Heeger A J 2010 Semiconducting polymers: the third generation *Chem. Soc. Rev.* **39** 2354
[2] Nelson J 2011 Polymer: fullerene bulk heterojunction solar cells *Mater. Today* **14** 462–70
[3] Blom P W M, Mihailetchi V D, Koster L J A and Markov D E 2007 Device physics of polymer: fullerene bulk heterojunction solar cells *Adv. Mater.* **19** 1551–66
[4] Karak S, Homnick P J, Renna L A, Venkataraman D, Mague J T and Lahti P M 2014 Solution-processed photovoltaics with a 3,6-Bis(diarylamino)fluoren-9-ylidene malononitrile *ACS Appl. Mater. Interfaces* **6** 16476–80
[5] Cui Y *et al* 2020 Single-junction organic photovoltaic cells with approaching 18% efficiency *Adv. Mater.* **32** 1–7
[6] Cui Y *et al* 2019 Wide-gap non-fullerene acceptor enabling high-performance organic photovoltaic cells for indoor applications *Nat. Energy* **4** 768–75
[7] Karak S, Liu F, Russell T P and Duzhko V V 2014 Bulk charge carrier transport in push-pull type organic semiconductor *ACS Appl. Mater. Interfaces* **6** 20904–12
[8] Karak S, Homnick P J, Della Pelle A M, Bae Y, Duzhko V V, Liu F, Russell T P, Lahti P M and Thayumanavan S 2014 Crystallinity and morphology effects on a solvent-processed solar cell using a triarylamine-substituted squaraine *ACS Appl. Mater. Interfaces* **6** 11376–84
[9] Pareek S, Waheed S, Rana A, Sharma P and Karak S 2020 Graphitic carbon nitride quantum dots (g-C_3N_4) to improve photovoltaic performance of polymer solar cell by

combining Förster resonance energy transfer (FRET) and morphological effects *Nano Express* **1** 010057
[10] Krebs F C 2009 Fabrication and processing of polymer solar cells: A review of printing and coating techniques *Sol. Energy Mater. Sol. Cells* **93** 394–412
[11] Mazzio K A and Luscombe C K 2015 The future of organic photovoltaics *Chem. Soc. Rev.* **44** 78–90
[12] Mohammad T, Kumar V and Dutta V 2020 Spray deposited indium doped tin oxide thin films for organic solar cell application *Physica* E **117** 113793
[13] Bihar E, Corzo D, Hidalgo T C, Rosas-Villalva D, Salama K N, Inal S and Baran D 2020 Fully inkjet-printed, ultrathin and conformable organic photovoltaics as power source based on cross-linked PEDOT:PSS electrodes *Adv. Mater. Technol.* **2000226** 1–7
[14] Jiang Z, Rahmanian R, Soltanian S, Nouri R and Servati P 2019 Single-pass spray-coated flexible organic solar cells using graphene transparent electrodes *2019 IEEE Int. Flex. Electron. Technol. Conf. IFETC 2019* pp 15–16
[15] Destouesse E, Top M, Lamminaho J, Rubahn H G, Fahlteich J and Madsen M 2019 Slot-die processing and encapsulation of non-fullerene based ITO-free organic solar cells and modules *Flex. Print. Electron.* **4** 045004
[16] Eslamian M 2014 Spray-on thin film PV solar cells: advances, potentials and challenges *Coatings* **4** 60–84
[17] Azarova N A, Owen J W, McLellan C A, Grimminger M A, Chapman E K, Anthony J E and Jurchescu O D 2010 Fabrication of organic thin-film transistors by spray-deposition for low-cost, large-area electronics *Org. Electron.* **11** 1960–5
[18] Bernardin G A, Davies N A and Finlayson C E 2017 Spray-coating deposition techniques for polymeric semiconductor blends *Mater. Sci. Semicond. Process.* **71** 174–80
[19] Reale A, LaNotte L, Salamandra L, Polino G, Susanna G, Brown T M, Brunetti F and DiCarlo A 2015 Spray coating for polymer solar cells: an up-to-date overview *Energy Technol.* **3** 385–406
[20] Bose S, Keller S S, Alstrøm T S, Boisen A and Almdal K 2013 Process optimization of ultrasonic spray coating of polymer films *Langmuir* **29** 6911–9
[21] Girotto C, Rand B P, Genoe J and Heremans P 2009 Exploring spray coating as a deposition technique for the fabrication of solution-processed solar cells *Sol. Energy Mater. Sol. Cells* **93** 454–8
[22] Habibi M, Rahimzadeh A, Bennouna I and Eslamian M 2017 Defect-free large-area (25 cm^2) light absorbing perovskite thin films made by spray coating *Coatings* **7** 42
[23] Lee J, Sagawa T and Yoshikawa S 2013 Thickness dependence of photovoltaic performance of additional spray coated solar cells *Thin Solid Films* **529** 464–9
[24] Zheng Y, Li S, Yu X, Zheng D and Yu J 2014 Investigation of in-situ annealing on poly(3,4-ethylenedioxythiophene): poly(styrenesulfonate): towards all-solution-processed inverted polymer solar cells *RSC Adv.* **4** 16464–71
[25] Zheng Y, Wu R, Shi W, Guan Z and Yu J 2013 Effect of in-situ annealing on the performance of spray coated polymer solar cells *Sol. Energy Mater. Sol. Cells* **111** 200–5
[26] Waheed S, Pareek S, Singh P, Sharma P, Rana A and Karak S 2020 Effect of *in-situ* annealing on phase segregation and optoelectronic properties of ultrasonic-spray deposited polymer blend films *IEEE J. Photovolt.* **2020** 1–8
[27] Aziz F, Ismail A F, Aziz M and Soga T 2014 Effect of solvent annealing on the crystallinity of spray coated ternary blend films prepared using low boiling point solvents *Chem. Eng. Process. Process Intensif.* **79** 48–55
[28] Huang Y-C, Tsao C-S, Cha H-C, Chuang C-M, Su C-J, Jeng U-S and Chen C-Y 2016 Correlation between hierarchical structure and processing control of large-area spray-coated polymer solar cells toward high performance *Sci. Rep.* **6** 20062
[29] De Luca G, Treossi E, Liscio A, Mativetsky J M, Scolaro L M, Palermo V and Samorì P 2010 Solvent vapour annealing of organic thin films: controlling the self-assembly of functional systems across multiple length scales *J. Mater. Chem.* **20** 2493–8
[30] Eslamian M 2017 Excitation by acoustic vibration as an effective tool for improving the characteristics of the solution-processed coatings and thin films *Prog. Org. Coat.* **113** 60–73
[31] Rahimzadeh A and Eslamian M 2017 On evaporation of thin liquid films subjected to ultrasonic substrate vibration *Int. Commun. Heat Mass Transfer* **83** 15–22
[32] Prasad R and Dalvi S V 2020 Sonocrystallization: monitoring and controlling crystallization using ultrasound *Chem. Eng. Sci.* **226** 115911
[33] Rahimzadeh A and Eslamian M 2017 Experimental study on the evaporation of sessile droplets excited by vertical and horizontal ultrasonic vibration *Int. J. Heat Mass Transfer* **114** 786–95
[34] Wang Q and Eslamian M 2016 Improving uniformity and nanostructure of solution-processed thin films using ultrasonic substrate vibration post treatment (SVPT) *Ultrasonics* **67** 55–64
[35] Zabihi F and Eslamian M 2018 Effect of the ultrasonic substrate vibration on nucleation and crystallization of PbI2 crystals and thin films *Crystals* **8** 60
[36] Habibi M, Eslamian M, Soltani-Kordshuli F and Zabihi F 2016 Controlled wetting/dewetting through substrate vibration-assisted spray coating (SVASC) *J. Coat. Technol. Res.* **13** 211–25
[37] Xiong H, Zabihi F, Wang H, Zhang Q and Eslamian M 2018 Grain engineering by ultrasonic substrate vibration post-treatment of wet perovskite films for annealing-free, high performance, and stable perovskite solar cells *Nanoscale* **10** 8526–35
[38] Ahmadian-Yazdi M R, Habibi M and Eslamian M 2018 Excitation of wet perovskite films by ultrasonic vibration improves the device performance *Appl. Sci.* **8** 308
[39] Eslamian M and Zabihi F 2015 Ultrasonic substrate vibration-assisted drop casting (SVADC) for the fabrication of photovoltaic solar cell arrays and thin-film devices *Nanoscale Res. Lett.* **10** 1–5
[40] Zabihi F and Eslamian M 2016 Fundamental study on the fabrication of inverted planar perovskite solar cells using two-step sequential substrate vibration- assisted spray coating (2S-SVASC) *Nanoscale Res. Lett.* **11** 71
[41] Zabihi F and Eslamian M 2015 Characteristics of thin films fabricated by spray coating on rough and permeable paper substrates *J. Coat. Technol. Res.* **12** 489–503
[42] Zabihi F and Eslamian M 2015 Substrate vibration-assisted spray coating (SVASC): significant improvement in nano-structure, uniformity, and conductivity of PEDOT:PSS thin films for organic solar cells *J. Coat. Technol. Res.* **12** 711–9
[43] Chandrasekaran N, Gann E, Jain N, Kumar A, Gopinathan S, Sadhanala A, Friend R H, Kumar A, McNeill C R and Kabra D 2016 Correlation between photovoltaic performance and interchain ordering induced delocalization of electronics states in conjugated polymer blends *ACS Appl. Mater. Interfaces* **8** 20243–50
[44] Shen Q *et al* 2015 Optical absorption, charge separation and recombination dynamics in Sn/Pb cocktail perovskite solar cells and their relationships to photovoltaic performances *J. Mater. Chem.* A **3** 9308–16
[45] Mihailetchi V D, Koster L J A, Hummelen J C and Blom P W M 2004 Photocurrent generation in

polymer-fullerene bulk heterojunctions *Phys. Rev. Lett.* **93** 19–22
[46] Shrotriya V, Yao Y, Li G and Yang Y 2006 Effect of self-organization in polymer/fullerene bulk heterojunctions on solar cell performance *Appl. Phys. Lett.* **89** 1–4
[47] Spano F C, Clark J, Silva C and Friend R H 2009 Determining exciton coherence from the photoluminescence spectral line shape in poly(3-hexylthiophene) thin films *J. Chem. Phys.* **130** 074904
[48] Brown P J, Thomas D S, Köhler A, Wilson J S, Kim J-S, Ramsdale C M, Sirringhaus H and Friend R H 2003 Effect of interchain interactions on the absorption and emission of poly(3-hexylthiophene) *Phys. Rev.* B **67** 064203
[49] Rahimzadeh A, Ahmadian-Yazdi M R and Eslamian M 2018 Experimental study on the characteristics of capillary surface waves on a liquid film on an ultrasonically vibrated substrate *Fluid Dyn. Res.* **50** 065510